Local mode behavior in the acetylene bending system

Matthew P. Jacobson, Robert J. Silbey, and Robert W. Field

Citation: J. Chem. Phys. **110**, 845 (1999); doi: 10.1063/1.478052
View online: http://dx.doi.org/10.1063/1.478052
View Table of Contents: http://jcp.aip.org/resource/1/JCPSA6/v110/i2
Published by the American Institute of Physics.

Local mode behavior in the acetylene bending system

Matthew P. Jacobson,[a] Robert J. Silbey, and Robert W. Field
Department of Chemistry and George R. Harrison Spectroscopy Laboratory, Massachusetts Institute of Technology, Cambridge, Massachusetts 02139

(Received 26 June 1998; accepted 5 October 1998)

The bending eigenfunctions of the acetylene $\tilde{X}^1\Sigma_g^+$ state, as represented by our recently reported effective Hamiltonian [J. Chem. Phys. **109**, 121 (1998)], are analyzed up to $E_{\mathrm{vib}}=15\,000\ \mathrm{cm}^{-1}$. A transition from normal to local mode behavior is observed around 8000–10 000 cm^{-1}, such that above these energies, the eigenstates are better described in terms of local mode quantum numbers. The local mode behavior in the bend degrees of freedom of acetylene that is described here is in many ways analogous to the local mode behavior that has been observed in the stretching degrees of freedom of many ABA molecules. However, the local mode behavior in the acetylene bend degrees of freedom, because it involves two two-dimensional rather than two one-dimensional vibrational modes, encompasses a richer range of motions. Specifically, in the ''local'' limit, the bending eigenfunctions are describable in terms of a continuum of motions ranging from local bend (one hydrogen bending) to counter-rotation (the two hydrogens executing rotations in opposite directions). © *1999 American Institute of Physics.* [S0021-9606(99)00702-3]

I. INTRODUCTION

The quantum vibrational eigenfunctions of polyatomic molecules at chemically significant energies are a subject of substantial recent interest, particularly insofar as they may provide mechanistic insights into unimolecular dissociation and isomerization. It is well established, at this point, that traditional spectroscopic analyses, which emphasize assignments based on normal modes, are rarely useful for describing large amplitude vibrational motions of polyatomic molecules. The nonlinearity and nonintegrability that are inherent to these large amplitude vibrations often lead to the observation of stable motions qualitatively distinct from the normal modes, as well as to classical chaos (and, possibly, observable quantum manifestations of the chaos). Some recent contributions to the understanding of the vibrational eigenfunctions of highly excited polyatomics have included:

(i) the fitting and analysis of effective Hamiltonian models which represent large amplitude motions;[1–5]
(ii) classical and semiclassical analysis of molecular quantum Hamiltonians;[6–12]
(iii) theoretical studies of vibrational eigenfunctions at high energy using potential surfaces generated by *ab initio* methods;[13,14]
(iv) algebraic approaches to molecular vibrations;[15–18]
(v) the polyad formalism for identifying approximately conserved vibrational quantum numbers;[19–22]
(vi) quantum, semiclassical, and classical studies of model systems which mimic important properties of polyatomic systems;[23–25]
(vii) detailed analysis of the equivalence[2,26–32] between the traditional normal mode models of vibrational motion and the local mode models pioneered by Mecke, Siebrand, Williams, Henry, Lawton, Child, and others;[33–38]

as well as a wide variety of experimental studies, which are far too numerous to be referenced here.

We present here, as a contribution to this body of literature, a thorough analysis of the bending eigenfunctions of the acetylene $\tilde{X}^1\Sigma_g^+$ state, as represented by an effective Hamiltonian model which has been demonstrated to reproduce all relevant experimental data up to 15 000 cm^{-1} of internal energy, with $\pm 1.4\ \mathrm{cm}^{-1}$ accuracy[1] (our approach to obtaining the eigenfunctions from experimental spectra is outlined in Sec. II). The eigenfunctions at such high internal energy necessarily represent rather large amplitude bending motions; 15 000 cm^{-1} corresponds to approximately 22 quanta of bending excitation, and is also believed to be within $\sim$2000 cm^{-1} of the energy at which acetylene is capable of isomerizing to vinylidene (zero-point dressed barrier height).[39–44] Although we believe that these high energy eigenfunctions may provide insights into quantum manifestations of classical chaos, we will not pursue this direction here, choosing instead to focus on the appearance of qualitatively new, stable bending motions at high internal energy. (A classical and semiclassical study of the acetylene bending system has recently been completed which addresses the correspondence between the quantum wave functions and classical periodic orbits and chaos[45]).

The new bending motions that are observed in highly vibrationally excited acetylene can be referred to as ''local bend'' and ''counter-rotation'' motions. Local bend motions have been reported previously in classical, semiclassical, and quantum studies of acetylene.[6,46,47] We are unaware of any previous characterization of the counter-rotating motion. The primary goal of this paper, however, is to demonstrate that the appearance of *both* the local bend *and* the counter-rotating motions can be considered a manifestation of a tran-

[a]Electronic mail: jacobson@mit.edu

sition from normal to local mode behavior in the bending dynamics. That is, while a normal mode basis set is appropriate at low energies (below $\sim$8000 cm^{-1}), a local mode basis becomes a superior zero-order representation at higher energies (above $\sim$10 000 cm^{-1}). The local mode behavior that we report here for the bending degrees of freedom of acetylene has obvious parallels with the local mode behavior which has been extremely well characterized for the stretching dynamics of a wide variety of ABA molecules (as well as some larger systems).[2,26,28,34,48–50] However, it should be kept in mind that the acetylene bending system has a higher dimensionality than the stretching systems of ABA molecules, leading to a rich range of behaviors for which the conventional language of local stretching systems is not entirely appropriate.

II. DETERMINING EIGENFUNCTIONS FROM SPECTRA

Our approach to determining the eigenfunctions of acetylene from experimental spectra consists of several steps:

(1) Dispersed fluorescence (DF) spectra are recorded from several vibrational levels of the $\tilde{A}^1A_u$ state of acetylene and subjected to frequency and intensity calibration.
(2) Numerical pattern recognition algorithms are used to extract from the DF data set the fractionation patterns for single bright states.
(3) An effective Hamiltonian (H^{eff}) model is fit to the set of extracted fractionated bright states.
(4) The eigenfunctions of the H^{eff} model are examined graphically in an appropriate coordinate system.

It should be noted that this approach is similar in spirit to that of a few other studies, including the Sako and Yamanouchi study of SO_2[15] and the Ishikawa *et al.* study of HCP,[3] but the tetra-atomic system under study here has required a more elaborate analysis. Steps (1), (2), and (3) of the procedure have been documented elsewhere.[1,51] Here we review only a few key concepts involved in the analysis of the DF spectra, primarily to introduce notation that will be used throughout this paper.

Our analysis of the DF spectra is made possible by the existence of three approximately conserved, *polyad* quantum numbers in the acetylene ground electronic state.[19–22] The polyad quantum numbers are:

$$N_{\text{res}}=5v_1+3v_2+5v_3+v_4+v_5, \tag{1}$$

$$N_s=v_1+v_2+v_3, \tag{2}$$

and

$$l=l_4+l_5. \tag{3}$$

The physical meanings of the N_s and l quantum numbers are simple; they represent the total number of quanta of stretching excitation and the total vibrational angular momentum,[52] respectively. The N_{res} quantum number has a slightly more subtle meaning; it reflects the approximate ratios among the normal mode frequencies, and thus represents a (de facto) restriction under which only states with approximately the same zero-order energy interact.

One important subset of the polyads that we have observed experimentally are those with $N_s=0$ (zero quanta of stretch excitation), the so-called pure bending polyads, for which the N_{res} quantum number simplifies to

$$N_{\text{res}}=v_4+v_5=N_b. \tag{4}$$

Here we have introduced N_b, the number of quanta of bending excitation, as a shorthand notation for the N_{res} and N_s polyad numbers for the pure bending polyads. It should also be noted that g/u symmetry is conserved by all resonances in a $D_{\infty h}$ molecule, and thus can also be used to label vibrational levels, as well as the rigorously conserved total angular momentum quantum number J and parity, which can be labeled using either the $\pm$ or e/f conventions. Thus, to identify a pure bending polyad uniquely, a total of five labels must be specified: N_b, l, J, g/u, and parity. In the discussion below, we will restrict our attention to $J=0$, and identify polyads using the shorthand notation $[N_b,l]^{g+}$.

The pure bending polyads that are observed experimentally have $g/+$ parity, and $6\leqslant N_b\leqslant 22$. Two classes of rotational lines, which terminate on $(J=1, l=0)$ and $(J=2, l=2)$, are observed. To model these data, we have refined and extended previously reported H^{eff} models for the acetylene bending system[53–55] to fit all available experimental data up to 15 000 cm^{-1} with ± 1.4 cm^{-1} accuracy. We will designate our acetylene pure bending effective Hamiltonian as $H^{\text{eff}}_{\mathcal{N}}$, in which the $\mathcal{N}$ subscript indicates that the effective Hamiltonian is represented in a normal mode basis, to distinguish it from an equivalent local mode version of the Hamiltonian ($H^{\text{eff}}_{\mathcal{L}}$) to be defined in Sec. VI. The matrix elements of $H^{\text{eff}}_{\mathcal{N}}$ are listed elsewhere;[1] here we will represent $H^{\text{eff}}_{\mathcal{N}}$ in a somewhat different form. Specifically, to anticipate algebraic manipulation of $H^{\text{eff}}_{\mathcal{N}}$ in later sections, we express it entirely in terms of raising and lowering operators for the two-dimensional (2D) isotropic harmonic oscillator. These operators are labeled d and g, using the notation of Cohen–Tannoudji *et al.*,[56] and are defined as

$$\hat{a}_d=\frac{1}{\sqrt{2}}(\hat{a}_x-i\hat{a}_y), \tag{5}$$

$$\hat{a}_g=\frac{1}{\sqrt{2}}(\hat{a}_x+i\hat{a}_y), \tag{6}$$

where x/y represent the two equivalent rectilinear coordinates for the 2D oscillator. The d/g operators have the convenient property that the number operators corresponding to the conventional quantum number labels for the 2D oscillator can be expressed as

$$\hat{v}=\hat{v}_d+\hat{v}_g=\hat{a}_d^{\dagger}\hat{a}_d+\hat{a}_g^{\dagger}\hat{a}_g, \tag{7}$$

$$\hat{l}=\hat{v}_d-\hat{v}_g=\hat{a}_d^{\dagger}\hat{a}_d-\hat{a}_g^{\dagger}\hat{a}_g. \tag{8}$$

Using the conventional ''4'' and ''5'' labels for *trans* and *cis*, respectively,

$$\hat{H}^{\rm eff}_{\mathcal{N}} = \omega_4\hat{v}_4 + \omega_5\hat{v}_5 + x_{44}\hat{v}_4\hat{v}_4 + x_{45}\hat{v}_4\hat{v}_5 + x_{55}\hat{v}_5\hat{v}_5 + y_{444}\hat{v}_4\hat{v}_4\hat{v}_4 + y_{445}\hat{v}_4\hat{v}_4\hat{v}_5 + y_{455}\hat{v}_4\hat{v}_5\hat{v}_5 + y_{555}\hat{v}_5\hat{v}_5\hat{v}_5 + g_{44}\hat{l}_4\hat{l}_4$$
$$+ g_{45}\hat{l}_4\hat{l}_5 + g_{55}\hat{l}_5\hat{l}_5 + s_{45}(\hat{a}^\dagger_{4d}\hat{a}^\dagger_{4g}\hat{a}_{5d}\hat{a}_{5g} + \hat{a}_{4d}\hat{a}_{4g}\hat{a}^\dagger_{5d}\hat{a}^\dagger_{5g}) + [r^\circ_{45} + r_{445}(\hat{v}_4 - 1) + r_{545}(\hat{v}_5 - 1)]$$
$$\times(\hat{a}_{4d}\hat{a}^\dagger_{4g}\hat{a}^\dagger_{5d}\hat{a}_{5g} + \hat{a}^\dagger_{4d}\hat{a}_{4g}\hat{a}_{5d}\hat{a}^\dagger_{5g}) + \tfrac{1}{4}[r^\circ_{45} + r_{445}(\hat{v}_4 - 1) + r_{545}(\hat{v}_5 - 1) + 2g_{45}]$$
$$*(\hat{a}^\dagger_{4d}\hat{a}^\dagger_{4d}\hat{a}_{5d}\hat{a}_{5d} + \hat{a}^\dagger_{4g}\hat{a}^\dagger_{4g}\hat{a}_{5g}\hat{a}_{5g} + \hat{a}_{4d}\hat{a}_{4d}\hat{a}^\dagger_{5d}\hat{a}^\dagger_{5d} + \hat{a}_{4g}\hat{a}_{4g}\hat{a}^\dagger_{5g}\hat{a}^\dagger_{5g}). \quad (9)$$

The values of the various parameters in this model[57] are listed in Table II of Ref. 1.

We evaluate $H^{\rm eff}_{\mathcal{N}}$, of course, in a product basis set of two 2D harmonic oscillators, which represent the *trans* and *cis* bend degrees of freedom. The existence of the polyad quantum numbers implies that the matrix representation of $H^{\rm eff}_{\mathcal{N}}$ is block diagonal. Upon diagonalization of any polyad block, the eigenvector matrix permits any eigenfunction in the polyad to be expressed as a linear superposition of the zero-order basis states, and the probability density for any given eigenfunction can be calculated in an appropriate set of coordinates. The most natural coordinates for the 2D isotropic harmonic oscillator are the radial and angular coordinates (ρ,ϕ), in which the wave functions for the oscillator take the form

$$\Psi_{v,l}(\rho,\phi) = \chi^{|l|}_v(\rho)e^{il\phi}, \quad (10)$$

$$\chi^{|l|}_v(\rho) = N_{v,|l|}e^{-\rho^2/2}\rho^{|l|}L^{|l|}_{(v+l)/2}(\rho^2), \quad (11)$$

where L represents the associated Laguerre polynomials, and N is a normalization constant. Note that the volume of integration in these coordinates is $\rho\, d\rho\, d\phi$.

A natural set of coordinates for the eigenstates of $H^{\rm eff}_{\mathcal{N}}$ is therefore $(\rho_4,\phi_4,\rho_5,\phi_5)$. We will restrict our discussion to eigenstates with $l=0$, in which case $l_4=-l_5$, and the basis set consists of

$$\Psi^0_{v_4,v_5}(\rho_4,\rho_5) = \chi^0_{v_4}(\rho_4)\chi^0_{v_5}(\rho_5) \quad (12)$$

for $l_4=l_5=0$, and

$$\Psi^{l_4}_{v_4,v_5}(\rho_4,\rho_5,\Phi_{45}) = \chi^{|l_4|}_{v_4}(\rho_4)\chi^{|l_4|}_{v_5}(\rho_5)e^{il_4\Phi_{45}} \quad (13)$$

for $l_4\neq 0$, in which $\Phi_{45}=\phi_4-\phi_5$. Note, however, that the latter set of basis functions do not possess well-defined parity; symmetrized basis functions can be defined as:

$$\Psi^{|l_4|+}_{v_4,v_5}(\rho_4,\rho_5,\Phi_{45}) = \sqrt{2}\chi^{|l_4|}_{v_4}(\rho_4)\chi^{|l_4|}_{v_5}(\rho_5)\cos(l_4\Phi_{45}), \quad (14)$$

$$\Psi^{|l_4|-}_{v_4,v_5}(\rho_4,\rho_5,\Phi_{45}) = \sqrt{2}\chi^{|l_4|}_{v_4}(\rho_4)\chi^{|l_4|}_{v_5}(\rho_5)\sin(l_4\Phi_{45}). \quad (15)$$

Note that the conservation of vibrational angular momentum permits a reduction in the number of coordinates needed to plot the eigenstates from 4 to 3. Also note that the g/u symmetry of the basis functions is determined by v_5 (v_5=odd implies u symmetry; v_5=even implies g symmetry). We will use the shorthand notation $|v^{l_4}_4,v^{l_5}_5\rangle^{g^+}_{\mathcal{N}}$ to indicate the symmetrized basis functions; the superscript, of course, indicates the symmetry, while the subscript $\mathcal{N}$ again indicates the normal mode basis set, to distinguish it from the local mode basis set to be defined in Sec. IV.

III. EIGENFUNCTIONS IN NORMAL MODE COORDINATES

We begin our discussion of the bending eigenfunctions of acetylene with a comparison between a set of eigenfunctions belonging to the $[4,0]^{g^+}$ (Fig. 1) and $[22,0]^{g^+}$ (Fig. 2) polyads. The $[4,0]^{g^+}$ polyad is representative of the low energy polyads ($N_b\leqslant 8$), in which the eigenfunctions can be rationalized simply in terms of perturbations/mixings among

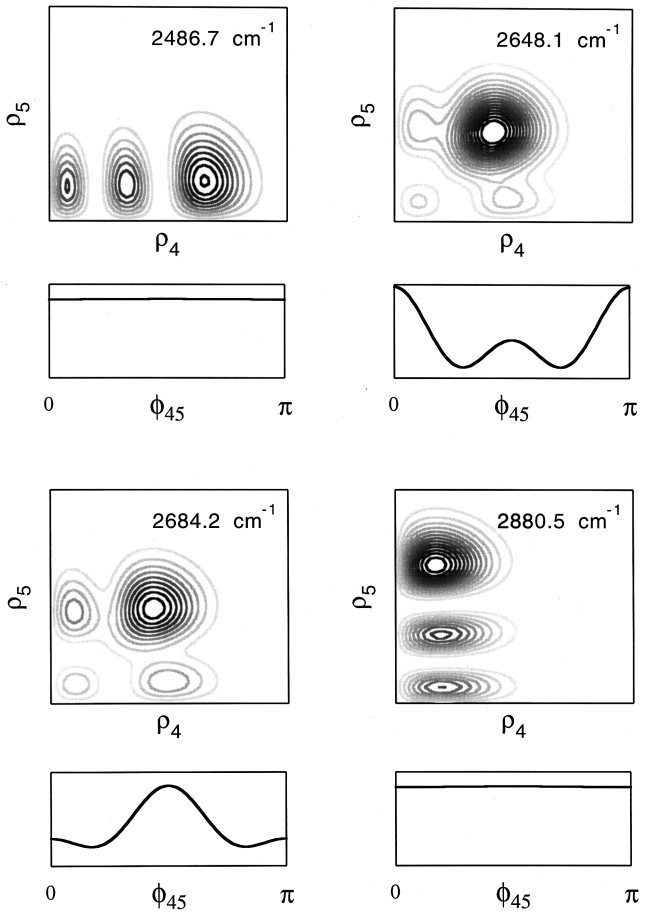

FIG. 1. Probability densities of the four eigenstates of the $[4,0]^{g^+}$ polyad plotted as projections onto the normal mode radial (ρ_4,ρ_5) and torsional (Φ_{45}) coordinates. The lowest energy eigenstate is a minimally perturbed *trans* bend state ($|4^0,0^0\rangle^{g^+}_{\mathcal{N}}$), and the highest a minimally perturbed *cis* bend state ($|0^0,4^0\rangle^{g^+}_{\mathcal{N}}$). The two eigenstates which are intermediate in energy are mixed, due to vibrational l-resonance between $|2^{+2},2^{-2}\rangle^{g^+}_{\mathcal{N}}$ and $|2^0,2^0\rangle^{g^+}_{\mathcal{N}}$.

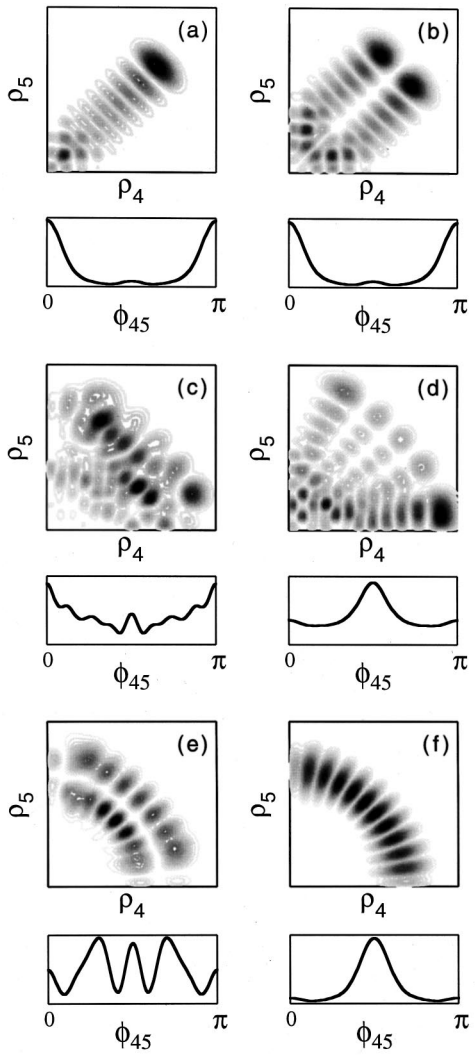

FIG. 2. Probability densities of six eigenstates in the $[22,0]^{g+}$ polyad plotted as projections onto the normal mode radial (ρ_4,ρ_5) and torsional (Φ_{45}) coordinates. The eigenstate in (a) has the lowest eigenenergy within the polyad (13 925.4 cm^{-1}) and eigenstate (b) has the third lowest (14 064.32 cm^{-1}). Together, (a) and (b) are representative of the eigenfunctions at the bottom of the polyad, which tend to have probability localized near $\rho_4=\rho_5$. The eigenfunction in (c) has an energy of 14 641.4 cm^{-1} and is representative of a number of eigenstates within the middle of the polyad which appear to have no well-defined nodal coordinates. Eigenstate (d) is depicted because it has the greatest overlap with the bright state (i.e., the greatest intensity in the experimental spectrum); its energy is 14 755.0 cm^{-1}. Eigenstates (e) and (f) are representative of many states at the top of the polyad, which tend to have nodal coordinates along lines of constant $(\rho_4^2+\rho_5^2)$. Eigenstate (e) has an energy of 15 067.6 cm^{-1} and (f) has an energy of 15 671.4 cm^{-1}, the highest eigenenergy within the polyad.

a small number of normal mode zero-order states. The $[22,0]^{g+}$ polyad is the highest energy pure bending polyad that has been characterized experimentally at this point. The eigenstates of this polyad have energies near 15 000 cm^{-1} and are representative of the high energy polyads ($18\leqslant N_b\leqslant 22$), in which few, if any, states are describable in terms of the normal mode basis, but are describable instead in terms of qualitatively new types of motions, which we call local bend and counter-rotation. We defer to Sec. V any discussion of the eigenfunctions at intermediate energy ($10\leqslant N_b\leqslant 16$), which are transitional between the low and high energy extremes.

The $[4,0]^{g+}$ polyad encompasses a total of four eigenstates, which are represented in Fig. 1 in the coordinates defined in Sec. II. The four zero-order states that comprise the polyad are $|4^0,0^0\rangle_{\mathcal{N}}^{g+}$, $|2^0,2^0\rangle_{\mathcal{N}}^{g+}$, $|2^{+2},2^{-2}\rangle_{\mathcal{N}}^{g+}$, and $|0^0,4^0\rangle_{\mathcal{N}}^{g+}$, and the projections of the eigenstates onto the basis set can be obtained from the eigenvector matrix which results from the diagonalization of $H_{\mathcal{N}}^{\text{eff}}$. Eigenfunction (a) is the minimally perturbed pure *trans* bend zero-order state, $|4^0,0^0\rangle_{\mathcal{N}}^{g+}$. That is, this lowest energy eigenstate within the polyad has 99.1% character of $|4^0,0^0\rangle_{\mathcal{N}}^{g+}$ (we use the term ''character'' to mean overlap squared between an eigenstate and a given zero-order function). The purity of this state is reflected in the eigenfunction plot; there is a clear nodal coordinate[58] running nearly parallel to the ρ_4 axis, and a nearly flat Φ_{45} probability distribution, which is indicative of $l_4=l_5=0$. The assignment for eigenstate (d), the highest energy state within the polyad, is equally clear [99.2% $|0^0,4^0\rangle_{\mathcal{N}}^{g+}$ character].

The two eigenstates in the ''middle'' of the polyad, by process of elimination, must correspond in some way to the $|2^0,2^0\rangle_{\mathcal{N}}^{g+}$ and $|2^{+2},2^{-2}\rangle_{\mathcal{N}}^{g+}$ zero-order states. Note that the $|2^0,2^0\rangle_{\mathcal{N}}^{g+}$ zero-order state should have a flat Φ_{45} probability distribution, while $|2^{+2},2^{-2}\rangle_{\mathcal{N}}^{g+}$ should have a $\cos^2(2\Phi_{45})$ distribution. Since neither of the eigenstates displays either of these behaviors, they must represent some mixture of the two zero-order states (i.e., the zero-order states perturb each other significantly). The eigenvector matrix confirms this conclusion. Eigenstate (b) can be approximated as $|b\rangle\approx 0.80|2^{+2},2^{-2}\rangle_{\mathcal{N}}^{g+}+0.60|2^0,2^0\rangle_{\mathcal{N}}^{g+}$, while for eigenstate (c), $|c\rangle\approx 0.60|2^{+2},2^{-2}\rangle_{\mathcal{N}}^{g+}-0.79|2^0,2^0\rangle_{\mathcal{N}}^{g+}$. The mechanism for the mixing between the two zero-order states is vibrational *l*-resonance, which couples states with the same v_4 and v_5, but with $\Delta l_4=-\Delta l_5=2$.

Thus, the overall structure of the pure bending polyads at low internal energy is fairly simple. The *trans* bend mode has a smaller harmonic frequency than the *cis* bend mode ($\omega_4<\omega_5$) and as a result, the states within the polyad are ordered with the pure *trans* bend state at the bottom, the pure *cis* bend state at the top, and states with a mixture of *trans* and *cis* in the middle. Groups of zero-order states with the same v_4 and v_5 tend to cluster closely in energy, due to the rather weak dependence of the zero-order energies on l_4 and l_5, and perturb each other strongly through vibrational *l*-resonance. By contrast, the other important anharmonic bending resonances, Darling-Dennison I and II, which couple states with $\Delta v_4=-\Delta v_5=2$, result in relatively minor perturbations, due to the fairly large difference in the frequencies of the two bending modes.

The situation in the $[22,0]^{g+}$ polyad is drastically different. At ~15 000 cm^{-1} of internal energy, this polyad not only encompasses many more zero-order states (42) than the low energy polyads, but these zero-order states are also coupled by off-diagonal matrix elements which are much larger due to their (harmonic oscillator) scaling properties. In addition, as we demonstrated in previous work,[1] the energies of the zero-order states do not cluster in a simple fashion, as

they do at low energy. Although the pure *cis* bend zero-order state, $|0^0,22^0\rangle_{\mathcal{N}}^{g+}$, retains the highest energy within the polyad, the pure *trans* bend state, $|22^0,0^0\rangle_{\mathcal{N}}^{g+}$, no longer has the lowest energy in the polyad, as it does for the low energy polyads. In fact, the $|22^0,0^0\rangle_{\mathcal{N}}^{g+}$ state has the fourth highest zero-order energy within the polyad, and the pure *trans* and *cis* bend states are thus nearly isoenergetic at high N_b. The underlying reason for this behavior is that the *trans* and *cis* bend modes have anharmonicities with opposite signs. The *trans* bend mode, which has a lower harmonic frequency, has a *positive* anharmonicity, which causes the effective frequency for this mode at high energy to approach that of the *cis* bend mode, which has a higher harmonic frequency but a negative anharmonicity.

Based on the preceding observations, it is not surprising that the eigenvector matrix for this polyad reveals that the vast majority of eigenstates can only be described in terms of a complicated superposition of many normal mode states (see for instance the histogram plot of dilution factors for this polyad in Fig. 4 of Ref. 1). On this basis, one might reasonably expect that the majority of the eigenfunctions of the $[22,0]^{g+}$ polyad would look very complicated in a graphical representation, with poorly defined nodal patterns. However, as Fig. 2 makes clear, many of the eigenfunctions of the $[22,0]^{g+}$ polyad demonstrate simple, well-defined nodal coordinates. Figures 2(a), 2(b), 2(e), and 2(f) are representative of the eigenstates at the low and high energy extremes of the polyad, the majority of which have clearly defined nodal coordinates.[59] Although many of the eigenstates in the middle of the polyad, like eigenstate (c), do have complicated structures, some states, like eigenstate (d), have well-defined nodal coordinates (although somewhat more complicated than at the energy extremes).

It should be emphasized that the eigenfunctions which have a simple appearance are also highly mixed, in the sense that their projection onto the normal mode basis set involves a complicated superposition of all of the zero-order states within the polyad. That is, their simple nodal coordinates are very different than those observed at low internal energy, where the eigenstates can be identified as perturbed/mixed normal mode zero-order states, with the nodal coordinates aligned approximately parallel to the ρ_4 and ρ_5 axes. Put differently, the simple eigenfunctions which predominate at the extremes of the $[22,0]^{g+}$ polyad represent qualitatively new motions which are not present at low internal energy.

It is clear that the eigenfunctions at the high and low energy extremes of the polyad represent two different types of motion. The motion associated with eigenstate (a), the lowest energy eigenstate within the polyad, is somewhat easier to interpret. This eigenfunction has its probability density localized around $\Phi_{45}=0$, which corresponds to in-plane motion. The nodal coordinate in the (ρ_4,ρ_5) plane is aligned along $\rho_4=\rho_5$. Classically, the simultaneous excitation of the *cis* and *trans* bending motions with the same amplitude, in phase and in plane, corresponds to a ''local bending'' motion, in which only *one* hydrogen executes a bending motion. From a quantum mechanical perspective, the bending motions of the two equivalent hydrogens are indistinguishable, and one would expect to observe a nearly degenerate *pair* of local bend states which correspond to positive and negative superpositions of the two equivalent local bend motions. In fact, eigenstate (a), which has a computed energy of 13 925.941 760 36 $cm^{-1}$and $g/+$ symmetry, is very nearly degenerate with an eigenstate of the $[22,0]^{u+}$ block of $H_{\mathcal{N}}^{\text{eff}}$, with a computed energy of 13 925.941 760 29 cm^{-1}(splitting of 7×10^{-7} cm^{-1}). The probability density plots of these two eigenfunctions are also nearly identical. Thus, in close analogy to local stretch states, the local bend states that we observe as eigenfunctions of $H_{\mathcal{N}}^{\text{eff}}$ appear in nearly degenerate g/u pairs.

Many of the eigenstates at the low energy end of the polyad can be classified as local benders, such as eigenstate (b), which differs from (a) in that it also involves excitation along a coordinate orthogonal to the local bending coordinate. As expected, this $g/+$ symmetry eigenstate, which has an energy of 14 064.322 161 5 cm^{-1}, has a nearly degenerate $u/+$ symmetry partner, only 3×10^{-6} cm^{-1} higher in energy. Several other g/u local bend pairs can be identified at the low energy end of the polyad, including pairs with $-$ parity. All of these states share a nodal coordinate aligned approximately along $\rho_4=\rho_5$, but many of these, such as (b), also have excitation along an orthogonal coordinate or have probability distributions which are not localized around $\Phi_{45}=0$. Further discussion of these other local bend states will be deferred to Sec. IV, in which we introduce a different coordinate representation of the eigenfunctions which makes their assignments more readily apparent.

The motion associated with eigenstate (f), the highest energy eigenstate within the polyad, is somewhat more difficult to interpret. The nodes of this eigenfunction align along a coordinate defined by $\sqrt{\rho_4^2+\rho_5^2}\approx C$, where C is a constant, and the probability density peaks at $\Phi_{45}=\pi/2$. The absence of substantial probability near $(\rho_4=0,\rho_5=0)$ implies that the motion never passes through the linear configuration. On the other hand, the motion must pass through the *trans* and *cis* planar configurations, due to the lobes of probability located near $\rho_4=0$ (with nonzero displacement in ρ_5) and $\rho_5=0$ (with nonzero displacement in ρ_4). The point $\rho_4=\rho_5$, with $\Phi_{45}=\pi/2$, corresponds to a configuration of the molecule in which the two hydrogens are located at the same angle with respect to the CC axis, and have a torsional angle between them of 90° [note that Φ_{45} is *not*, however, the torsional angle between the hydrogens, but the torsional angle between the *cis* and *trans* oscillators, as discussed in Sec. IV]. In this way, it becomes clear that a trajectory along the coordinate $\sqrt{\rho_4^2+\rho_5^2}=C$, with $\Phi_{45}=\pi/2$, corresponds to a molecular motion in which the two hydrogens maintain a given angle with respect to the CC axis, but execute an internal rotation which changes the torsional angle between them. Since total vibrational angular momentum must be conserved, the two hydrogens execute rotations in the opposite sense, and thus we identify eigenstate (f) with a counter-rotating motion.

In contrast to the local bend states, counter-rotating states do not appear in g/u pairs with the same parity. However, eigenstate (f), which has $g/+$ parity and an energy of 15 671.432 833 cm^{-1}, is very nearly degenerate with an eigenstate of the $u/-$ symmetry block of $H_{\mathcal{N}}^{\text{eff}}$, which has an

energy of 15 671.432 824 cm^{-1} (splitting of 1.2×10^{-5} cm^{-1}). A number of the other states at the high energy end of the polyad which have nodal coordinates along $\sqrt{\rho_4^2+\rho_5^2}=C$, such as eigenstate (e), also appear in pairs of either $g/+$ with $u/-$, or $g/-$ with $u/+$. That is, the counter-rotation states occur in pairs with opposite g/u symmetry *and* opposite parity. This behavior can be rationalized as follows. Classically, there are two equivalent counter-rotations, which differ in the direction of rotations of the hydrogens (i.e., clockwise or counterclockwise). Quantum mechanically, these classical counter-rotations, like the classical local bends, are indistinguishable, and the nearly perfect quantum counter-rotation states such as eigenstate (f) must represent some superposition of the two equivalent motions.

To make this discussion more concrete, we designate the two equivalent classical counter-rotations as $(\mathcal{R},\mathcal{L})$ and $(\mathcal{L},\mathcal{R})$, where $\mathcal{R}$ and $\mathcal{L}$ represent clockwise and counterclockwise rotation of one hydrogen. The application of the molecular inversion operator $(\hat{i})$ to either classical counter-rotation state generates the other, i.e.,

$$\hat{i}(\mathcal{R},\mathcal{L})\rightarrow(\mathcal{L},\mathcal{R}).$$

The application of the parity operator, which for a symmetric top is equivalent to $\hat{\sigma}_v$ (see, for instance, Refs. 60 and 61), has an identical effect:

$$\hat{\sigma}_v(\mathcal{R},\mathcal{L})\rightarrow(\mathcal{L},\mathcal{R}).$$

Thus, upon symmetrizing the equivalent counter-rotation states,

$$\frac{1}{\sqrt{2}}[(\mathcal{R},\mathcal{L})\pm(\mathcal{L},\mathcal{R})],$$

it becomes clear that the positive superposition corresponds to $g/+$ symmetry, while the negative superposition corresponds to $u/-$ symmetry. Thus, while local bend states appear in pairs with opposite g/u symmetry, because $\hat{i}$ interchanges the two equivalent local bends ($\hat{\sigma}_v$ is inoperative), counter-rotation states appear in pairs with opposite g/u symmetry *and* opposite parity, because *both* $\hat{i}$ and $\hat{\sigma}_v$ interchange the two equivalent counter-rotations.

At this point, we have not yet discussed in detail eigenfunctions (c) and (d). There is little to say about eigenstate (c), except that no simple nodal coordinates can be identified, despite a significant degree of localization of probability density around $\Phi_{45}=0$. The existence of an eigenfunction with such a complicated appearance raises suspicions that chaos exists in the underlying classical dynamics, at least in the middle of the polyad; this is, in fact, the case, and the intricate coexistence of regular and chaotic regions of phase space for the acetylene bending system at high internal energy will be examined in a future publication.[45] Eigenstate (d), on the other hand, is representative of a number of eigenstates in the middle of the polyad which have a fairly regular structure (some degree of counter-rotating character is evident). It also has the special significance of being the eigenstate on which the strongest transition to the $[22,0]^{g+}$ polyad terminates in our DF spectra. The substantial overlap of this eigenstate with the pure *trans* bend bright state is evident in the accumulation of probability density near $\rho_5=0$.

IV. EIGENFUNCTIONS REPRESENTED IN LOCAL MODE COORDINATES

On the basis of the preceding arguments, it is clear that many of the eigenfunctions at the low and high energy ends of the $[22,0]^{g+}$ polyad should be assignable in terms of quantum numbers representing excitation along local bend and counter-rotation coordinates. We define in this section a coordinate transformation from the $(\rho_4,\rho_5,\Phi_{45})$ normal mode coordinates, which were utilized to represent the eigenfunctions in Sec. III, to a new set of coordinates, $(\rho_A,\rho_B,\Phi_{AB})$, which facilitate the assignment of many of the high energy eigenstates in terms of ''local mode'' quantum numbers. This coordinate transformation, and the assignments that it permits, also provide insight into the relationship that exists between the local bend and counter-rotating motions, as well as the significance of the ''imperfect'' local bend and counter-rotation states, such as eigenstates (b) and (e).

Although we have plotted the wave functions in radial coordinates, we define the coordinate transformation in dimensionless rectilinear coordinates as:

$$q_{Ax}=\frac{1}{\sqrt{2}}(q_{4x}+q_{5x}), \tag{16}$$

$$q_{Ay}=\frac{1}{\sqrt{2}}(q_{4y}+q_{5y}), \tag{17}$$

$$q_{Bx}=\frac{1}{\sqrt{2}}(-q_{4x}+q_{5x}), \tag{18}$$

$$q_{By}=\frac{1}{\sqrt{2}}(-q_{4y}+q_{5y}). \tag{19}$$

The coordinates A and B are thus defined to be symmetric and antisymmetric combinations of the *trans* and *cis* bend coordinates, and we will refer to these new coordinates as ''local mode'' bending coordinates, in the expectation that they represent, to a good approximation, bending coordinates for the two individual hydrogens (the correspondence between the normal and local mode representations of the bend eigenfunctions is established more rigorously in Sec. VI). Upon transforming to radial coordinates, the local and normal mode coordinates are related according to

$$\rho_A^2=\tfrac{1}{2}[\rho_4^2+\rho_5^2+2\rho_4\rho_5\cos(\Phi_{45})], \tag{20}$$

$$\rho_B^2=\tfrac{1}{2}[\rho_4^2+\rho_5^2-2\rho_4\rho_5\cos(\Phi_{45})], \tag{21}$$

$$\Phi_{AB}=\arctan\left(\frac{2\rho_4\rho_5\sin(\Phi_{45})}{\rho_5^2-\rho_4^2}\right). \tag{22}$$

These expressions are invertible. Note that Φ_{AB} is easier to interpret than Φ_{45};Φ_{AB} is simply the torsional angle between the two hydrogens.

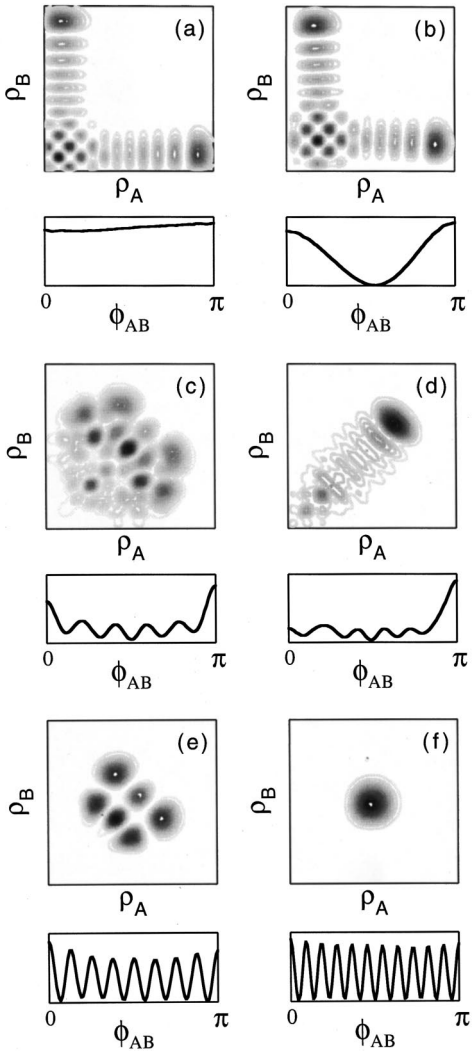

FIG. 3. The same eigenfunctions as in Fig. 2, but plotted using local mode coordinates. ρ_A and ρ_B are the two equivalent single hydrogen bending coordinates, and Φ_{AB} is the torsional angle between the hydrogens.

The application of this coordinate transformation to the eigenfunctions of Fig. 2 is depicted in Fig. 3. In order to provide assignments for the eigenfunctions in the local mode coordinate system, we define a zero-order basis set of two 2D harmonic oscillators, which is analogous to the normal mode basis set defined in Eqs. (12)–(15) above:

$$\Psi^0_{v_A,v_B}(\rho_A,\rho_B)=\chi^0_{v_A}(\rho_A)\chi^0_{v_B}(\rho_B) \tag{23}$$

for $l_A=l_B=0$, and

$$\Psi^{|l_A|+}_{v_A,v_B}(\rho_A,\rho_B,\Phi_{AB})=\sqrt{2}\chi^{|l_A|}_{v_A}(\rho_A)\chi^{|l_A|}_{v_B}(\rho_B)\cos(l_A\Phi_{AB}), \tag{24}$$

$$\Psi^{|l_A|-}_{v_A,v_B}(\rho_A,\rho_B,\Phi_{AB})=\sqrt{2}\chi^{|l_A|}_{v_A}(\rho_A)\chi^{|l_A|}_{v_B}(\rho_B)\sin(l_A\Phi_{AB}) \tag{25}$$

as the positive and negative parity pairs for $l_A\neq 0$. One important distinction from the normal mode basis set is that the local mode basis, as defined above, does not have well-defined g/u symmetry. This can be remedied by taking positive and negative superpositions of $\Psi^{|l_A|}_{v_A,v_B}$ and $\Psi^{|l_A|}_{v_B,v_A}$ ($v_A\neq v_B$). The set of local mode basis functions with $g/+$ symmetry, for instance, is then defined as

$$\Psi^{|l_A|g+}_{v_A,v_B}(\rho_A,\rho_B,\Phi_{AB})=[\chi^{|l_A|}_{v_A}(\rho_A)\chi^{|l_A|}_{v_B}(\rho_B)+\chi^{|l_A|}_{v_B}(\rho_A)\chi^{|l_A|}_{v_A}(\rho_B)]\cos(l_A\Phi_{AB}). \tag{26}$$

We will use the shorthand notation $|v_A^{l_A},v_B^{l_B}\rangle^{g+}_{\mathcal{L}}$ for the fully symmetrized local mode basis functions.

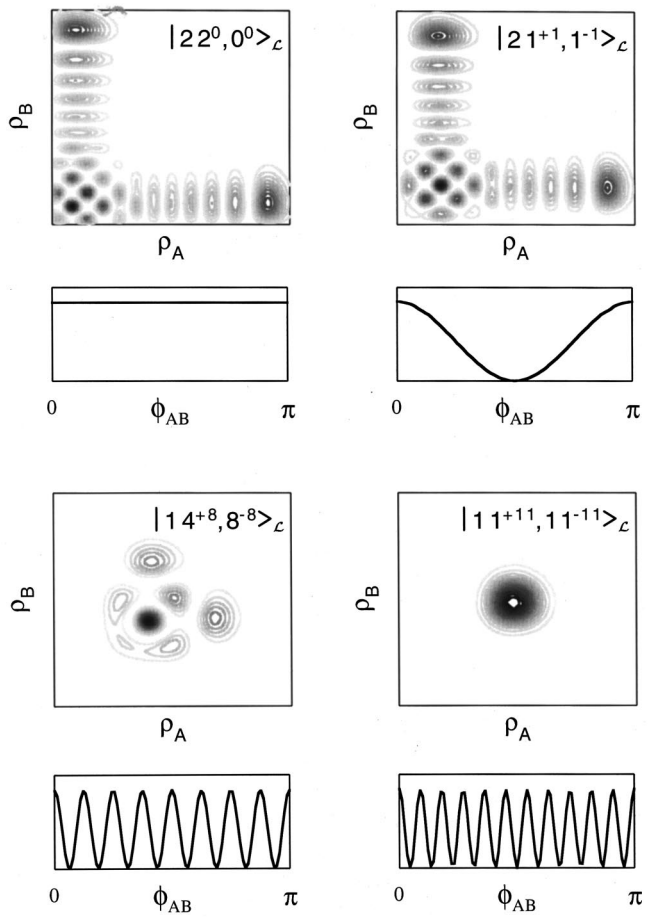

FIG. 4. Probability densities of four symmetrized local mode basis functions, $|v_A^{l_A},v_B^{l_B}\rangle^{g+}_{\mathcal{L}}$. Note the similarity between these zero-order states and eigenfunctions (a), (b), (e), and (f) in Fig. 3.

Plotted in Fig. 4 are four of these basis functions; their correspondence with the eigenstates (a), (b), (e), and (f) in Fig. 3 is clear. Eigenstate (a) can be identified as $|22^0,0^0\rangle^{g+}_{\mathcal{L}}$; it has probability localized along *both* $\rho_A=0$ and $\rho_B=0$, the two equivalent local bending coordinates, because of the indistinguishability of the two hydrogens in quantum mechanics. Eigenstate (b) can be identified as $|21^{+1},1^{-1}\rangle^{g+}_{\mathcal{L}}$. Note that the single, nearly sinusoidal oscillation of the probability density from 0 to π along Φ_{AB} is indicative of a single quantum of angular momentum in the local bending modes (i.e., $l_A=-l_B=1$). The assignment of eigenstate (e) as $|14^{+8},8^{-8}\rangle^{g+}_{\mathcal{L}}$ is somewhat more approximate, but the number of oscillations in the Φ_{AB} coordinate matches exactly ($l_A=-l_B=8$), and the number and location of the nodes in

the radial coordinates are quite similar. Finally, the highest energy eigenstate within the polyad, eigenstate (f), can be assigned as $|11^{+11},11^{-11}\rangle_{\mathcal{L}}^{g+}$. That is, the counter-rotating states correspond to local mode basis functions with maximal or nearly maximal angular momentum associated with each of the individual bond oscillators.

Thus, the local mode basis set that we have defined in this section appears to be extremely useful for assigning acetylene bending vibrational levels at high internal energy, because *both* local bend *and* counter-rotation states can be labeled with the same set of quantum numbers. More precisely, the local mode basis set represents a continuum of vibrational character, ranging from pure local bend, $|N_b^0,0^0\rangle_{\mathcal{L}}$, to pure counter-rotation, $|N_b/2^{(N_b/2)}, N_b/2^{(-N_b/2)}\rangle_{\mathcal{L}}$. Most of the states near the bottom of the polyad, with $v_A \gg v_B$, lie close to the local bend limit, whereas the assignable states near the top of the polyad, with $v_A \approx v_B \approx |l_A|$, lie close to the counter-rotation limit. As will be seen in Sec. VI, nearly half of the eigenstates of the [22,0] polyad (of all symmetries) can be assigned using the local mode basis set (using the Hose-Taylor criterion[62]), especially those states at the high and low energy ends of the polyad, but a few in the middle as well. Many other eigenstates can be rationalized in terms of mixings among a few zero-order local mode states.

V. TRANSITION FROM NORMAL TO LOCAL MODE BEHAVIOR

It should be clear at this point that the bending eigenfunctions of acetylene in the limits of low (i.e., $N_b=4$) and high ($N_b=22$) excitation are strikingly different. At low energy, the eigenfunctions can be assigned in terms of perturbed or mixed normal mode states. At high energy, a few eigenfunctions have very complicated nodal patterns (in any coordinate set) which do not yield to assignment, but many others have well-defined, simple nodal coordinates corresponding to a continuum of new types of vibrational motions, ranging from local bend to counter-rotation. In this section we examine the transition between the low energy, normal mode regime, and the high energy, local mode regime.

To focus this discussion, we restrict our attention to the lowest and highest energy eigenstates in each pure bending polyad. As discussed in Sec. III, at low N_b, the lowest energy eigenstates in the pure bending polyads can be labeled as minimally perturbed *trans* bend states, while the highest eigenstates are nearly pure *cis* bend states. At high N_b, the lowest energy eigenstate is a local bender, while the highest is a counter-rotator. Thus, we can expect the change from normal to local mode behavior to be manifested in a dual transition, from *trans* bend to local bend behavior at the bottom of the pure bending polyads, and from *cis* bend to counter-rotation at the top (although it is unclear at this point whether these two transitions will necessarily occur at the same energy).

The symmetry properties of the local bend and counter-rotation states provide one method of identifying the energies at which these two transitions occur. That is, as detailed in Sec. III, pure local bend states are expected to appear in nearly degenerate $(g/+,u/+)$ pairs, while pure counter-rotation states should occur in $(g/+,u/-)$ pairs; no such symmetry arguments can be made for purely normal mode states. The second column in Table I is the difference in energy between the lowest energy eigenstates in corresponding $g/+$ and $u/+$ polyads. For $[6,0]^{g+}$, $[8,0]^{g+}$, and $[10,0]^{g+}$, in which the lowest energy eigenstate can be described as a perturbed *trans* bend state, the g/u energy splitting is >10 cm^{-1}. For $N_b>12$, however, the energy splitting is less than 1 cm^{-1}, and by $N_b=22$, the energy splittings become exceedingly small, indicating nearly perfect local bend character.[63] The third column of Table I is the energy difference between the highest energy eigenstates in corresponding $g/+$ and $u/-$ polyads. The transition from *cis* bend to counter-rotating behavior appears to occur somewhere around $N_b=16$.

TABLE I. Tabulation of energy splittings which reveal the transition from normal to local mode behavior. First column: the polyad quantum number, N_b. In all cases, $l=0$. Second column: energy difference, in cm^{-1}, between the lowest energy eigenstates in pairs of corresponding $g/+$ and $u/+$ symmetry polyads. Small splittings indicate that the states are assignable as local bends. Third column: energy difference between the highest energy eigenstates in pairs of corresponding $g/+$ and $u/-$ symmetry polyads. Small splittings indicate that the states are assignable as counter-rotators.

N_b	$E_{g+}-E_{u+}$	$E_{g+}-E_{u-}$
6	-52.2	83.2
8	-30.8	67.3
10	-10.3	48.1
12	-0.22	25.1
14	-1.7×10^{-4}	5.5
16	4.4×10^{-6}	0.39
18	6.5×10^{-7}	1.5×10^{-2}
20	1.2×10^{-7}	4.1×10^{-4}
22	6.4×10^{-8}	9.3×10^{-6}

Thus, the bottom of the pure bending polyads seems to demonstrate local mode behavior at slightly lower energy than the top; despite this fairly minor difference, it seems reasonable to conclude that the transition from normal to local mode behavior occurs within the range $N_b=12-16$ ($\sim$8 000–10 000 cm^{-1}). To examine this transition in greater detail, we plot the lowest and highest energy eigenstates of the pure bending polyads in the critical energy range in Figs. 5 and 6. Specifically, Fig. 5 depicts the lowest energy eigenstates in the $[10,0]^{g+}$, $[12,0]^{g+}$, and $[14,0]^{g+}$ polyads in both the normal and local mode coordinates that were defined previously. The lowest energy eigenstate in the $[10,0]^{g+}$ polyad can be observed to be a somewhat perturbed *trans* bend state in either of the coordinate sets. In the normal mode coordinates, the assignment of the eigenstate as $|10^0,0^0\rangle_{\mathcal{N}}^{g+}$ is indicated by the nodal coordinate in the (ρ_4,ρ_5) plane being nearly parallel to the ρ_4 axis, and by the nearly isotropic distribution of probability density along the Φ_{45} coordinate. In the local mode coordinates, the accumulation of probability along $\rho_A=\rho_B$ indicates that both hydrogens execute equal amplitude motions, and the probability maximum at $\Phi_{AB}=\pi$ indicates that the two hydrogens bend in opposite directions (i.e., *trans* as opposed to *cis*).

The lowest energy eigenstate in the $[12,0]^{g+}$ polyad, on

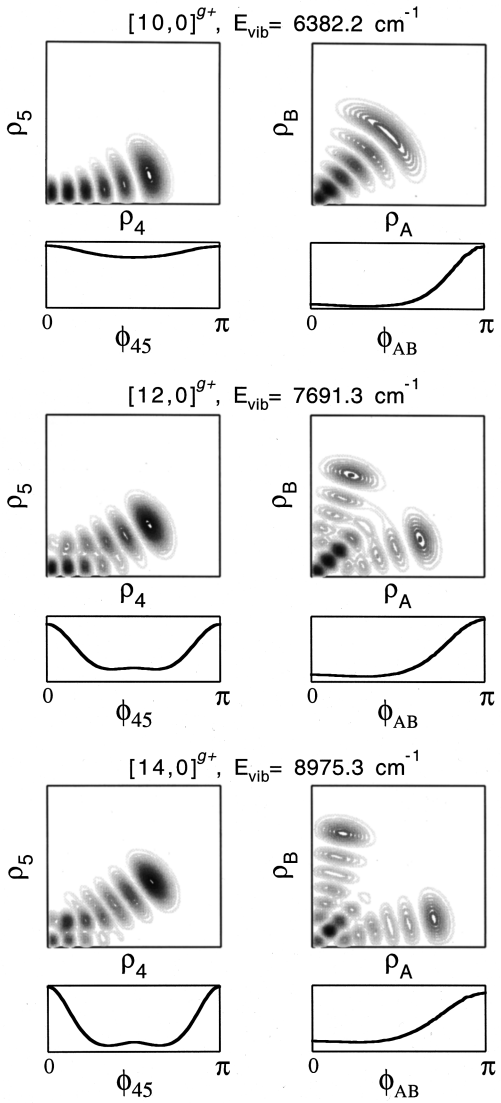

FIG. 5. The lowest energy eigenstates in the $[10,0]^{g+}$, $[12,0]^{g+}$, and $[14,0]^{g+}$ polyads, in normal and local mode bending coordinates. The qualitative change in eigenstate character from *trans* bend to local bend is clear at $N_b=12$. In the normal mode coordinates, the nodal coordinate in the (ρ_4,ρ_5) plane pulls away from the ρ_4 axis, and the torsional probability distribution begins to show pronounced peaks at $\Phi_{45}=0,\pi,\cdots$. In the local mode coordinates, the transition to local bend behavior is marked by the splitting of the probability in the (ρ_A,ρ_B) plane into two lobes.

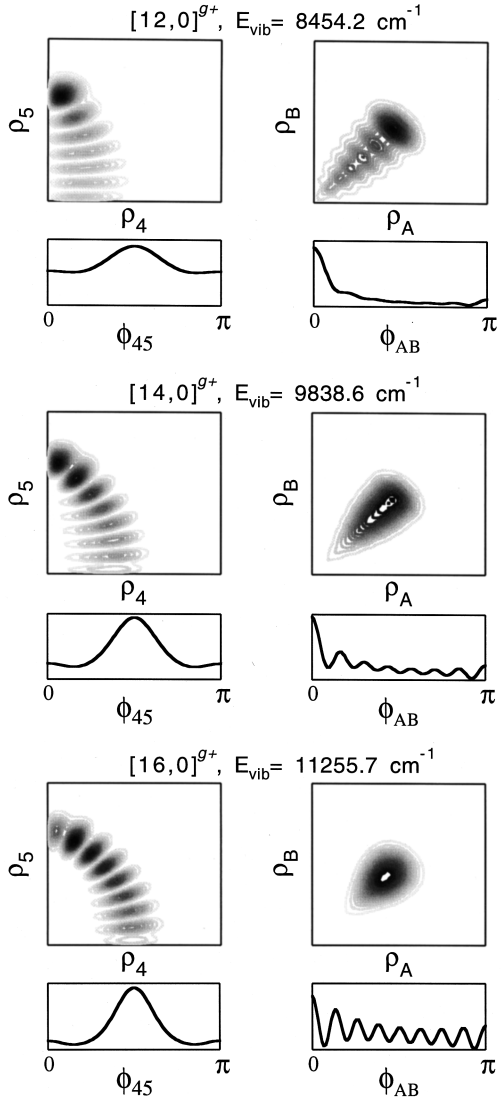

FIG. 6. The highest energy eigenstates in the $[12,0]^{g+}$, $[14,0]^{g+}$, and $[16,0]^{g+}$ polyads, in normal and local mode bending coordinates. The qualitative change in eigenstate character from *cis* bend to counter-rotating is clear at $N_b=14$. In the normal mode coordinates, the nodal coordinate in the (ρ_4,ρ_5) plane pulls away from the ρ_5 axis, and the torsional probability distribution begins to show a pronounced peak at $\Phi_{45}=\pi/2$. In the local mode coordinates, the transition to counter-rotating behavior is marked by the disappearance of the probability near $(\rho_A=0,\rho_B=0)$, and the development of well-defined oscillations in probability along the Φ_{AB} coordinate.

the other hand, displays several features which indicate a qualitatively new type of motion, and cannot be considered to represent merely a perturbed *trans* bend state. First, in the normal mode coordinates, the nodal coordinate in the (ρ_4,ρ_5) plane is no longer even approximately parallel to the ρ_4 axis. The probability density along the Φ_{45} coordinate for the $[12,0]^{g+}$ eigenstate also displays pronounced maxima at 0 and π which are nearly absent in the $[10,0]^{g+}$ eigenstate. The transition to a qualitatively new type of motion (which will eventually come to represent the local bend motion) is perhaps the clearest in the local bend coordinates. Specifically, the single nodal coordinate in the $[10,0]^{g+}$ eigenstate appears to have bifurcated in the $[12,0]^{g+}$ eigenstate to form a *pair* of nodal coordinates located symmetrically about $\rho_A=\rho_B$.

The lowest energy eigenstate in the $[14,0]^{g+}$ polyad displays no qualitative features that are not already present in the $[12,0]^{g+}$ lowest energy eigenstate. In fact, from $N_b=12$ to $N_b=22$, the change in the nature of the lowest energy eigenfunctions represents a gradual evolution toward the nearly perfect local bending motion associated with the lowest energy eigenstate in the $[22,0]^{g+}$ polyad. In the (ρ_4,ρ_5) plane, the nodal coordinate gradually increases its slope until it reaches (nearly) unity, and the probability maxima at $\Phi_{45}=0,\pi,\ldots$ become more pronounced. In the local mode coordinates, the two symmetrically related lobes of probability gradually move ''outward'' until they are approximately orthogonal and run parallel to the ρ_A and ρ_B axes. This is perhaps the clearest indicator of the increasing

''purity'' of the local bend motion. The $\rho_A=\rho_B$ direction represents equal amplitude motions of the two hydrogens, while the ρ_A and ρ_B axes represent the motion of just one hydrogen, with the other hydrogen held stationary at 0°. Thus, the migration of probability away from $\rho_A=\rho_B$, and towards $\rho_A=0$ and $\rho_B=0$, is a clear indication of the change in behavior from *trans* bend to local bend.

Having characterized the transition from *trans* bend to local bend character at the bottom of the pure bending polyads, we now turn to the corresponding transition at the top of the polyads, from *cis* bend to counter-rotating. Figure 6 depicts the highest energy eigenfunctions in the $[12,0]^{g+}$, $[14,0]^{g+}$, and $[16,0]^{g+}$ polyads. The highest energy eigenfunction in the $[12,0]^{g+}$ polyad appears to be describable as a *cis* bend state. In the normal mode coordinates, most of the probability in the (ρ_4,ρ_5) plane remains localized near the ρ_5 axis, and the probability distribution over the torsional coordinate Φ_{45} is fairly uniform, despite a slight bulge at $\Phi_{45}=\pi/2$. In the $[14,0]^{g+}$ polyad, however, the probability distribution of the lowest energy eigenstate in the (ρ_4,ρ_5) plane has ''pulled away'' from the ρ_5 axis, and the torsional probability distribution has become much more strongly peaked at $\Phi_{45}=\pi/2$. In the local mode coordinates, the most significant change in the probability distribution between $N_b=12$ and 14 is that in the $[14,0]^{g+}$ eigenstate, there is little probability density in the vicinity of $(\rho_A=0,\rho_B=0)$, indicating that the eigenstate is associated with a motion that never passes through the linear configuration.

Thus, we identify the lowest energy eigenstate in $[14,0]^{g+}$ as the first that clearly demonstrates a motion that is qualitatively different from *cis* bending, and demonstrates the first signatures of counter-rotating character. In $[16,0]^{g+}$, the counter-rotating character becomes more clear, with the nodal coordinate in the (ρ_4,ρ_5) plane beginning to approach the form of a semicircle (as it is for the nearly perfect counter-rotating states in $[22,0]^{g+}$). Further, the probability density in the (ρ_A,ρ_B) plane begins to resemble a minimum uncertainty Gaussian, indicating that the hydrogens are becoming locked into a given angle with respect to the CC axis. Finally, the probability distribution along the Φ_{AB} torsional coordinate develops well-defined oscillations (in this case, a total of eight), which indicate the number of quanta of angular momenta associated with each hydrogen.

One of the most interesting conclusions which arises from the preceding analysis is that the transition from *trans* to local bend character at the bottom of the polyad, and from *cis* to counter-rotating at the top, is *abrupt*, in the sense that a single eigenstate can be identified in which the first features of a qualitatively new motion are observed. Figure 7 provides an additional perspective on this phenomenon. Plotted in the figure is the energy difference between the lowest (circles) and highest (crosses) energy eigenstates in adjacent $(\Delta N_b=2)$ pure bending polyads. For $N_b\leqslant 10$, the highest energy eigenstates in each polyad are well approximated as pure *cis* bending states, and the lowest energy eigenfunctions as pure *trans* bending. Thus, the slopes of the two progressions of states can be explained trivially in terms of the opposite anharmonicities of the two normal modes. Above $N_b=10$ for the lower progression and $N_b=12$ for the upper

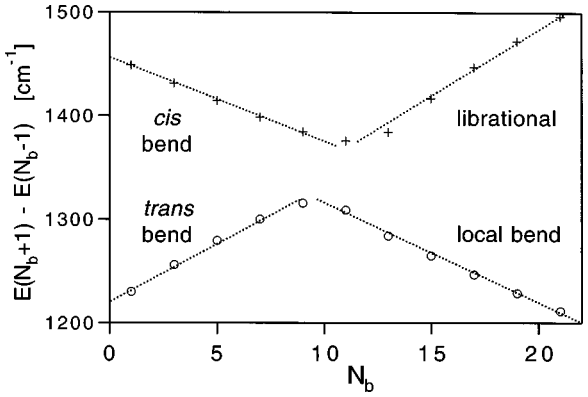

FIG. 7. Energy differences between the highest (crosses) and lowest (circles) energy eigenstates in adjacent $(\Delta N_b=2)$ pure bending polyads ($l=0$). The dotted lines are drawn for emphasis. The highest energy eigenstates within the polyads change character from *cis* bend to counter-rotation at $N_b\approx 14$, and the lowest energy eigenstates change character from *trans*-bend to local bend at $N_b\approx 12$.

progression, the slopes suddenly reverse. That is, the local bend and counter-rotating progressions of eigenfunctions appear rather suddenly, and can be characterized by positive and negative anharmonicities, respectively.

It should be noted that certain aspects of the analysis presented above have been noted previously in acetylene model systems as well as other Darling–Dennison systems. Sibert and McCoy reported[47,64] the existence of the local bending class of states in their adiabatic bending Hamiltonian, with properties similar to those reported here (although their calculations extended only to $\sim 10\,000$ cm^{-1}). (Local bend states were also reported in the earlier work of Sibert and Mayrhofer).[46] Sibert and McCoy do not, however, seem to have noted the existence of the counter-rotating states, perhaps because the counter-rotating states first appear at slightly higher internal energy than the local bend states.

In addition, Rose and Kellman have reported[6] an analysis of an earlier version of the acetylene H^{eff}, in which they also noted the existence of local bending eigenstates, as well as a set of eigenstates that they classified as ''precessional.'' It should be emphasized that the precessional states described by these authors do not, in fact, accurately represent any acetylene vibrational eigenstates. The precessional eigenstates differ from the counter-rotating states reported here in that they are implied to correspond to an in-plane motion, whereas the counter-rotating states only pass through planar configurations in a transitory way. The origin of this discrepancy is almost certainly due to the simplifying assumptions that Rose and Kellman invoked in order to facilitate the construction of a ''catastrophe map,'' namely their neglect of all of the resonances except Darling–Dennison Bend I. Ignoring this discrepancy, however, the catastrophe maps constructed by these authors do predict several of the qualitative trends observed here, such as the appearance of local benders at the bottom of the polyad, and precessional (counter-rotating) states at the top, as well as the initial appearance of local benders at a lower internal energy than the precessional (counter-rotating) states.

VI. LOCAL MODE REPRESENTATION OF ACETYLENE PURE BEND H^{eff}

In the preceding sections, we have demonstrated that, above $E_{\text{vib}} \approx 10\,000\ \text{cm}^{-1}$, many acetylene bending vibrational levels can be assigned using local bend quantum numbers. This analysis has been made possible by the $H_{\mathcal{N}}^{\text{eff}}$ which reproduces all of the relevant experimental data up to 15 000 cm^{-1}. Thus, a *normal* mode Hamiltonian has been used to investigate *local* mode behavior. There is nothing fundamentally wrong with such an approach; in a similar way, a model of Darling–Dennison coupled symmetric and antisymmetric stretches can be used to predict local stretching behavior.[26] However, the normal mode model provides little insight into the underlying physics of the local mode molecular vibrations. In this section, we define a local mode effective Hamiltonian $H_{\mathcal{L}}^{\text{eff}}$, which is related to $H_{\mathcal{N}}^{\text{eff}}$ by a unitary transformation, but which provides greater insight into the bending dynamics above $E_{\text{vib}} \approx 10\,000\ \text{cm}^{-1}$

There are a number of possible approaches to converting the bending effective Hamiltonian defined in Eq. (9) from the normal mode basis set to a local mode basis set. One of the most straightforward is a ''shift operator'' approach, which has been employed by Baggott,[2] Dellavalle,[32] Lehmann,[31] and others in studies of the equivalence of local and normal mode models for stretching systems. Briefly, raising and lowering operators can be defined for the local bend degrees of freedom in the same manner as for the normal modes. By applying the chain rule to the coordinate transformation defined in Eqs. (16)–(19), the normal and local mode raising/lowering operators are related to each other according to:

$$\hat{a}_{Ad} = \frac{1}{\sqrt{2}}(\hat{a}_{4d} + \hat{a}_{5d}), \tag{27}$$

$$\hat{a}_{Ag} = \frac{1}{\sqrt{2}}(\hat{a}_{4g} + \hat{a}_{5g}), \tag{28}$$

$$\hat{a}_{Bd} = \frac{1}{\sqrt{2}}(\hat{a}_{4d} - \hat{a}_{5d}), \tag{29}$$

$$\hat{a}_{Bg} = \frac{1}{\sqrt{2}}(\hat{a}_{4g} - \hat{a}_{5g}). \tag{30}$$

Using these relationships, the normal mode effective Hamiltonian $H_{\mathcal{N}}^{\text{eff}}$ can be transformed to an effective Hamiltonian in local mode coordinates $H_{\mathcal{L}}^{\text{eff}}$ using straightforward operator algebra.

We have carried out such a transformation but do not report it here because it is exceptionally tedious, and because the resultant local mode effective Hamiltonian, in and of itself, provides little additional insight into the underlying physics of the local mode behavior. Instead, we follow a more didactic approach, using earlier results of Lehmann,[65] who considered a simple local mode model Hamiltonian for the acetylene bend modes. In close analogy to the Child and Lawton[34] treatment of ABA local stretching systems, Lehmann defined a system of two identical, harmonically coupled two-dimensional oscillators, which can be represented by the following *local mode* effective Hamiltonian:

$$\begin{aligned}\hat{H}_{\mathcal{L}}^{\text{model}} = {} & \omega(\hat{v}_A + 1) + \omega(\hat{v}_B + 1) + x(\hat{v}_A + 1)^2 \\ & + x(\hat{v}_B + 1)^2 + g\hat{l}_A^2 + g\hat{l}_B^2 \\ & + \lambda(\hat{a}_{Ad}\hat{a}_{Bd}^\dagger + \hat{a}_{Ad}^\dagger\hat{a}_{Bd} + \hat{a}_{Ag}\hat{a}_{Bg}^\dagger + \hat{a}_{Ag}^\dagger\hat{a}_{Bg})\end{aligned} \tag{31}$$

(for acetylene, it can be demonstrated[65] that $x \approx -3g$). This simple model Hamiltonian is capable of representing both local and normal mode behavior, as well as intermediate cases. The local mode limit is achieved trivially when $\lambda = 0$ (i.e., when there is no coupling between the oscillators) or more generally when the anharmonicity of individual bend modes ''quenches'' the interbend coupling. The normal mode limit is achieved if the anharmonicity of the individual oscillators is neglected.

Despite being a useful conceptual tool for understanding normal and local bend behavior in acetylene, $H_{\mathcal{L}}^{\text{model}}$ is much too simple to provide a quantitatively accurate representation of our experimental data. Lehmann examined the limitations of $H_{\mathcal{L}}^{\text{model}}$ by transforming it to a normal mode effective Hamiltonian $H_{\mathcal{N}}^{\text{model}}$ by applying the relationships in Eqs. (27)–(30):

$$\begin{aligned}\hat{H}_{\mathcal{N}}^{\text{model}} = {} & (\omega - \lambda)(\hat{v}_4 + 1) + (\omega + \lambda)(\hat{v}_5 + 1) + \frac{x}{2}(\hat{v}_4 + 1)(\hat{v}_4 + 1) + \frac{3x + g}{2}(\hat{v}_4 + 1)(\hat{v}_5 + 1) + \frac{x}{2}(\hat{v}_5 + 1)(\hat{v}_5 + 1) + \frac{g}{2}\hat{l}_4\hat{l}_4 \\ & + \frac{3g + x}{2}\hat{l}_4\hat{l}_5 + \frac{g}{2}\hat{l}_5\hat{l}_5 + \frac{x - g}{4}(\hat{a}_{4d}^\dagger\hat{a}_{4g}^\dagger\hat{a}_{5d}\hat{a}_{5g} + \hat{a}_{4d}\hat{a}_{4g}\hat{a}_{5d}^\dagger\hat{a}_{5g}^\dagger) + \frac{x - g}{4}(\hat{a}_{4d}\hat{a}_{4g}^\dagger\hat{a}_{5d}^\dagger\hat{a}_{5g} + \hat{a}_{4d}^\dagger\hat{a}_{4g}\hat{a}_{5d}\hat{a}_{5g}^\dagger) \\ & + \frac{x + g}{8}(\hat{a}_{4d}^\dagger\hat{a}_{4d}^\dagger\hat{a}_{5d}\hat{a}_{5d} + \hat{a}_{4g}^\dagger\hat{a}_{4g}^\dagger\hat{a}_{5g}\hat{a}_{5g} + \hat{a}_{4d}\hat{a}_{4d}\hat{a}_{5d}^\dagger\hat{a}_{5d}^\dagger + \hat{a}_{4g}\hat{a}_{4g}\hat{a}_{5g}^\dagger\hat{a}_{5g}^\dagger).\end{aligned} \tag{32}$$

This normal mode representation of the model Hamiltonian $H_{\mathcal{N}}^{\text{model}}$ can be seen to be similar in structure to the effective Hamiltonian used to fit the experimental data that is defined in Eq. (9) ($H_{\mathcal{N}}^{\text{eff}}$). All of the diagonal elements of $H_{\mathcal{N}}^{\text{model}}$ also appear in $H_{\mathcal{N}}^{\text{eff}}$ (although the treatment of zero-point energy is different[57]). In addition, there are precisely three anharmonic resonances which generate off-diagonal matrix elements in each Hamiltonian: Darling–Denison Bend I and II, and vibrational *l*-resonance.

Thus, $H_{\mathcal{N}}^{\text{model}}$ can be considered to be a special case of

TABLE II. Selected assignments of eigenstates in the local mode basis set, $|v_A^{l_A}, v_B^{l_B}\rangle_{\mathcal{L}}$. All energies are in units of cm^{-1}, and ''character'' refers to the projection squared of the eigenfunction onto the relevant local mode basis function. ''Perturbed'' indicates that no eigenstate can be assigned as a particular local mode function using the Hose–Taylor criterion, because the basis function is substantially perturbed. ''Does not exist'' indicates that the local mode basis function with the given symmetry does not exist.

	$g/+$ symmetry		$u/+$ symmetry		$g/-$ symmetry		$u/-$ symmetry	
Assignment	Energy	Character	Energy	Character	Energy	Character	Energy	Character
$\|0^0,22^0\rangle_{\mathcal{L}}$	13 925.9	99.1%	13 925.9	99.1%	does not exist		does not exist	
$\|1^{+1},21^{-1}\rangle_{\mathcal{L}}$	14 064.3	96.8%	14 064.3	96.8%	13 984.6	98.9%	13 984.6	98.9%
$\|2^0,20^0\rangle_{\mathcal{L}}$	14 035.6	62.2%	14 035.6	62.2%	does not exist		does not exist	
$\|2^{+2},20^{-2}\rangle_{\mathcal{L}}$	perturbed		perturbed		14 136.0	97.6%	14 136.0	97.6%
$\|4^0,18^0\rangle_{\mathcal{L}}$	14 119.8	50.8%	14 119.8	50.8%	does not exist		does not exist	
$\|6^{+6},16^{-6}\rangle_{\mathcal{L}}$	14 718.4	68.0%	14 724.4	54.7%	14 722.2	63.8%	14 724.6	59.1%
$\|7^{+7},15^{-7}\rangle_{\mathcal{L}}$	14 882.6	54.0%	perturbed		14 888.5	66.6%	14 882.3	55.7%
$\|8^{+8},14^{-8}\rangle_{\mathcal{L}}$	15 067.6	75.5%	15 053.4	50.1%	15 053.3	50.3%	15 067.4	77.8%
$\|9^{+9},13^{-9}\rangle_{\mathcal{L}}$	14 882.6	54.0%	perturbed		14 888.5	66.6%	14 882.3	55.7%
$\|10^{+10},12^{-10}\rangle_{\mathcal{L}}$	15 067.6	75.5%	15 053.4	50.1%	15 053.3	50.3%	15 067.4	77.8%
$\|11^{+9},11^{-9}\rangle_{\mathcal{L}}$	15 306.7	51.3%	does not exist		does not exist		15 306.6	51.4%
$\|11^{+11},11^{-11}\rangle_{\mathcal{L}}$	15 671.4	97.8%	does not exist		does not exist		15 671.4	97.8%

$H_{\mathcal{N}}^{\text{eff}}$, in which certain high order terms ($y_{444}, y_{445}, y_{455}, y_{555}, r_{445}, r_{545}$) are omitted, and the constants for many of the remaining terms are constrained in certain internal relationships (analogous to the *x-K* relationships[2,29–32] that have been derived for many types of local stretch systems). Lehmann provides a complete list of these *x-K* relationships (Table I of Ref. 65). Some of these relationships are approximately obeyed by the parameters in the fitted effective Hamiltonian $H_{\mathcal{N}}^{\text{eff}}$; for instance, the fitted values of r_{45} and s_{45} are -6.193 and -8.572, which agree modestly with the constraint implied by $H_{\mathcal{N}}^{\text{model}}$ that $r_{45}=s_{45}$. On the other hand, as Lehmann emphasizes, $H_{\mathcal{N}}^{\text{model}}$ also implies that $x_{44}=x_{55}$; the fitted constants ($x_{44}=3.483$ and $x_{55}=-2.389$) do not even have the correct relative signs.

The serious discrepancies between Lehmann's simple model Hamiltonian ($H_{\mathcal{N}}^{\text{model}}$) and the fitted spectroscopic Hamiltonian ($H_{\mathcal{N}}^{\text{eff}}$) imply that a more sophisticated local mode Hamiltonian (which we designate $H_{\mathcal{L}}^{\text{eff}}$) is necessary to represent accurately the bending system of acetylene (i.e., $H_{\mathcal{L}}^{\text{eff}}$ will include higher order diagonal and off-diagonal terms that are neglected in $H_{\mathcal{L}}^{\text{model}}$). One straightforward and exact way of developing such a model is to partition the fitted spectroscopic Hamiltonian according to

$$H_{\mathcal{N}}^{\text{eff}}=H_{\mathcal{N}}^{\text{model}}+H', \tag{33}$$

in which the H' term represents all of the deviations of the full molecular bending effective Hamiltonian $H_{\mathcal{N}}^{\text{eff}}$ from the model Hamiltonian $H_{\mathcal{N}}^{\text{model}}$. The matrix representations of $H_{\mathcal{N}}^{\text{model}}$ and $H_{\mathcal{L}}^{\text{model}}$ are related by a unitary transformation, which can be obtained by diagonalizing $H_{\mathcal{N}}^{\text{model}}$ with $\lambda=0$. This unitary transformation can then be applied to H' to obtain the matrix representation of $H_{\mathcal{L}}^{\text{eff}}$.[66]

The eigenvalues and eigenfunctions of $H_{\mathcal{N}}^{\text{eff}}$ and $H_{\mathcal{L}}^{\text{eff}}$ are, of course, identical. Since these two representations of the effective Hamiltonian are equivalent, either can be used to describe the bending system of acetylene. However, the dynamics and eigenfunctions will generally be more easily understood in the representation in which the basis set functions more closely approximate the eigenfunctions. We have already provided a wealth of anecdotal evidence in the preceding sections that the eigenfunctions of $H_{\mathcal{N}}^{\text{eff}}$ in $[22,0]^{g+}$ are more readily assignable in a local mode coordinate set, and in fact we have already succeeded in assigning several eigenstates at the low and high energy extremes of the polyad. The development of the local mode representation $H_{\mathcal{L}}^{\text{eff}}$ allows these assignments to be made more rigorously. The eigenvector matrix resulting from the diagonalization of $H_{\mathcal{L}}^{\text{eff}}$ allows one to determine the assignability of all states within the polyad in the local representation using some suitable criterion.

One such criterion has been proposed by Hose and Taylor,[62] which specifies that an eigenfunction is *assignable* if at least 50% of its character is attributable to a single basis function. Using this criterion, we can assign 65 eigenstates in the $[22,0]$ polyad, out of a total of 144 (including all four possible symmetries). A subset of these assignments is listed in Table II. By comparison, only two eigenstates in the $N_b=22$ polyad can be assigned *normal mode* quantum numbers using the Hose–Taylor criterion.[67]

The ability to assign nearly 50% of the eigenfunctions in the $[22,0]$ polyad in the local mode basis set strongly suggests that it provides a superior representation of the bending dynamics of acetylene at high internal energy, as opposed to the traditional normal mode basis set. The suitability of the local mode basis at high internal energy can also be illustrated graphically using a correlation diagram[34,68] like the one in Fig. 8. The lines in the diagram represent the state energies in the polyad in different limits. In the middle of the diagram are the eigenenergies, and at the far left and right are the zero-order energies of the normal mode and local mode basis sets, respectively. At positions intermediate between the eigenstate and basis state extremes, the energies are calculated by diagonalizing $H_{\mathcal{N}}^{\text{eff}}$ (left) or $H_{\mathcal{L}}^{\text{eff}}$ (right) with the off-diagonal elements multiplied by a scaling factor between 0 (the unperturbed basis set limit) and 1 (the eigenstate limit). The assignability of the eigenstates in a given basis set can be judged by the ease with which the curves can be

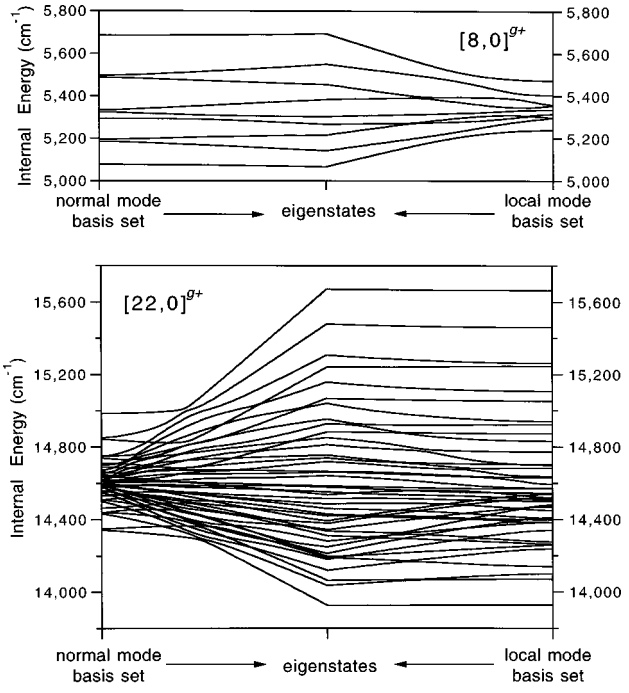

FIG. 8. Correlation diagrams for the normal and local mode basis sets for the $[8,0]^{g+}$ (top) and $[22,0]^{g+}$ (bottom) polyads. The lines in the diagram represent the state energies in the polyad in different limits. In the middle of the diagram are the eigenenergies, and at the far left and right are the zero-order energies of the normal mode and local mode basis sets, respectively. At positions intermediate between the eigenstate and basis state extremes, the energies are calculated by diagonalizing the effective Hamiltonian with the off-diagonal elements multiplied by a scaling factor between 0 (the unperturbed basis set limit) and 1 (the eigenstate limit). An eigenstate is likely to be assignable in terms of quantum numbers associated with a given basis set if the line which passes from the eigenstate to a zero-order basis state does so with minimal deviations, or can be followed through avoided crossings. It is clear from this diagram that many more eigenstates in the $[22,0]^{g+}$ polyad are assignable in the local mode basis set than in the traditional normal mode basis set, but that the normal mode basis set provides a better zero-order description of the eigenstates in the $[8,0]^{g+}$ polyad.

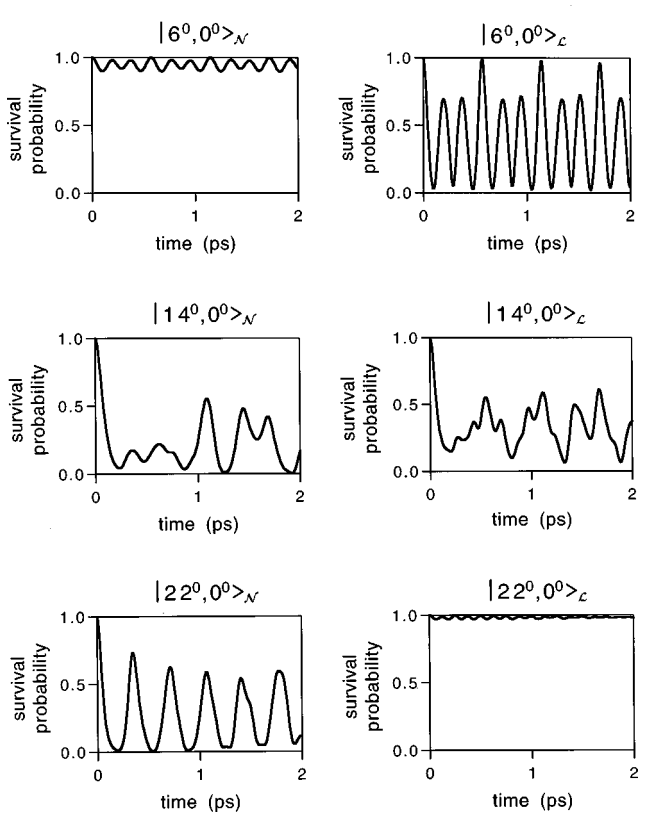

FIG. 9. Survival probabilities for selected zero-order states in the $[6,0]^{g+}$, $[14,0]^{g+}$, and $[22,0]^{g+}$ polyads. The left column contains the survival probabilities for pure *trans* bend zero-order states ($|N_b^0,0^0\rangle_{\mathcal{N}}^{g+}$), while the right column contains the survival probabilities for pure local bend zero-order states ($|N_b^0,0^0\rangle_{\mathcal{L}}^{g+}$). Exciting a local mode state in the normal mode (low energy) regime, or a normal mode state in the local mode (high energy) regime, results in strong, quasiperiodic oscillations in the survival probability. In the intermediate energy regime ($[14,0]^{g+}$), neither the local nor normal mode representations provide a simple way of conceptualizing the dynamics.

followed across avoided crossings from the eigenbasis to the zero-order basis.

This correlation diagram provides substantial evidence for the superiority of the local mode representation in the $[22,0]^{g+}$ polyad. Several of the energy curves correlate directly between the eigenbasis and the local mode zero-order basis without undergoing any anticrossings; the assignments of these eigenstates are trivial. Many other curves on the local mode side of the diagram can also be followed easily through a series of weakly avoided crossings. In contrast, on the normal mode side of the diagram, the energy dispersion of the zero-order basis set is much smaller than that of the eigenbasis, and thus the majority of the energy curves display strong curvature, which can be ascribed to multiple, long-range, avoided crossings. Put in a slightly different way, the local mode basis set provides a superior zero-order representation for the $[22,0]^{g+}$ polyad because the anharmonic resonances are weaker, in the sense that they mix the zero-order basis less strongly. In marked contrast, Fig. 8 also makes it clear that in the $[8,0]^{g+}$ polyad, the normal mode basis provides a better zero-order representation of the eigenfunctions, since the energy curves correlate much more simply with the normal mode than the local mode basis set.

Figure 9 illustrates how the local and normal mode representations of the effective Hamiltonian provide complementary insights into acetylene bending *dynamics*. Consider first the right-hand column, which depicts the survival probabilities for the series of pure local bend zero-order states, $|N_b^0,0^0\rangle_{\mathcal{L}}^{g+}$, in the $[6,0]^{g+}$, $[14,0]^{g+}$, and $[22,0]^{g+}$ polyads. The $|22^0,0^0\rangle_{\mathcal{L}}^{g+}$ zero-order state lies in the high energy, local mode regime, and is very nearly an eigenstate of the effective Hamiltonian. Thus, little energy flows from this state into any of the other states within the polyad. The behavior of the $|6^0,0^0\rangle_{\mathcal{L}}^{g+}$ zero-order state contrasts sharply. Energy flows rapidly from this state at early times, followed by a series of regular, strong recurrences. This is the expected behavior for a local mode excitation in the normal mode (low energy) regime. One can imagine a classical analog of this behavior in which one ''bends back'' one of the two hydrogens of the molecule; for a relatively small amplitude ''pluck,'' the bend excitation would oscillate back and forth between the two equivalent oscillators, since these oscillators exhibit strong coupling in the low energy limit.

Although the survival probabilities of the local bend zero-order states are useful for conceptualizing the bending

dynamics in the low and high energy regimes, the bright states that are actually observed in our experimental spectra are pure *trans* bend zero-order states, $|N_b^0,0^0\rangle_{\mathcal{N}}^{g^+}$. The survival probabilities for these bright states are plotted in the left hand column of Fig. 9, and the behavior of these states as a function of energy is essentially the opposite of that of the local bend states. In the low energy, normal mode regime ($|6^0,0^0\rangle_{\mathcal{N}}^{g^+}$), little energy exchange occurs, whereas the high energy, local mode regime ($|22^0,0^0\rangle_{\mathcal{N}}^{g^+}$) is characterized by strong, quasiperiodic oscillations in the survival probability. In the intermediate energy regime (i.e., $[14,0]^{g^+}$), in which the transition from normal to local mode behavior occurs, the survival probabilities of *both* the *trans* bend, $|14^0,0^0\rangle_{\mathcal{N}}^{g^+}$, and local bend, $|14^0,0^0\rangle_{\mathcal{L}}^{g^+}$, zero-order states evolve in a rather complicated manner, with fast initial decays ($\sim$100 fs) followed by a series of irregular partial recurrences. Thus, neither the local mode nor the normal mode paradigms provide simple insights into the dynamics in the complicated transitional regime. (In a forthcoming publication[45] it will be revealed that classical chaos plays a particularly important role at intermediate energies.)

We conclude this section by examining a weakness of the local mode effective Hamiltonian (and effective Hamiltonians in general), which is that it is difficult to relate the coordinate system that is implicit in the H^{eff} to a physical coordinate system of the molecule. As a consequence, it is not possible to *rigorously* determine, for instance, the maximum bend angle that is achieved in one of the local bend states, but a reasonable estimate is possible with a few assumptions. For concreteness, we consider the eigenstate depicted in Fig. 3(a), which can be assigned, to a very good approximation (see Table II) as $|22^0,0^0\rangle_{\mathcal{L}}^{g^+}$. We assume that the bending coordinate ρ_A (or equivalently ρ_B) is equivalent to the CCH bend angle (θ) of the molecule, i.e., that the local bend motion occurs with no change in the CH bond length. The force field of Bramley *et al.*[69] provides an excellent representation of the acetylene potential energy surface near equilibrium, and specifies the dependence of the potential energy on the bend angle as

$$V(\theta) = 6323 \cdot \theta^2 + 1110 \cdot \theta^4,$$

with V in units of cm^{-1}. Extrapolating this energy dependence to 19 675.9 cm^{-1} (the zero-point referenced eigenstate energy of 13 925.9 cm^{-1} plus an estimated 5750 cm^{-1} of zero-point energy), the classical turning point of the $|22^0,0^0\rangle_{\mathcal{L}}^{g^+}$ state is 1.49 rad (85.7°). Although this estimate of the classical turning point certainly cannot be considered quantitatively accurate, it is clear that the high-energy local bend states that we have considered in this paper involve very large amplitude motions.

VII. CONCLUSION

Using graphical and numerical evidence, we have argued for the appropriateness of a local mode representation of the bending system of acetylene at high vibrational energy ($E_{\text{vib}} > 10\,000$ cm^{-1}), in particular to describe the emergence of prominent local bend and counter-rotation states. On the other hand, we have also demonstrated that the conventional normal mode representation provides an adequate zero-order representation at low internal energy ($E_{\text{vib}} < 8000$ cm^{-1}) and studied in some detail the transition that occurs at intermediate energies from normal to local mode behavior. Thus, considerable insight is gained by describing the acetylene bending system with two formally equivalent but complementary representations; normal and local mode.

However, one can make the argument that the local mode model of acetylene bending dynamics is *globally* superior, in the sense that it provides greater insight into the underlying physics, in terms of simple, intuitive concepts such as momentum and potential coupling between bonds. Local mode formalisms, whether applied to stretches (as in many previous studies) or to bends (as we have done here) also have the advantage of permitting greater insight into trends among a series of molecules with similar structure or functionality. That is, normal mode models tend to be molecule specific, since every molecule has different normal modes, while local mode models are grounded in a valence bond mindset, which lies at the heart of qualitative chemical description.

There may also be a specific advantage to fitting acetylene ground state spectra using a local mode model (most previous fits[1,53–55] have used the traditional normal mode model). The coupling terms in a local mode model (off-diagonal elements) will be well determined by data at low energy (i.e., normal mode behavior dominates in the limit of strong coupling) while the bond anharmonicities (diagonal elements) will be well determined by data at high energy (i.e., local mode behavior dominates in the limit of strong bond anharmonicity). By contrast, in the normal mode model, high order terms both on and off diagonal are determined primarily by data at high energy (only the strongest anharmonic contributions are well determined at low internal energy). In addition, acetylene has long been known to display local stretch behavior (see, for instance, Ref. 34), and a fitting model which is local both in the stretches and bends may provide an optimal description of the molecule, especially at high energy.

We would also like to point out two other approaches to studying the acetylene bending system which may provide interesting perspectives that complement the work reported here. The first is the algebraic approach, which has been developed by Iachello, Levine, and others,[16,18] which may provide a deeper understanding of the equivalence of the normal and local perspectives presented in this work, as well as a more powerful way of treating mode anharmonicity. The second is the continuing development of potential surfaces for acetylene with spectroscopic accuracy. Normally, the refinement of a potential surface for a polyatomic molecule against experimental data to such high energy would be rather difficult, but the relatively low dimensionality of the acetylene bending system, together with the large amount of available data, should make such a refinement feasible (the work of Sibert and McCoy[47,64] provides an excellent starting point).

Finally, to end on a somewhat more speculative note, we wish to point out that the transition state for isomerization between acetylene and vinylidene is predicted by *ab initio* theory[39–41] to have a structure in which one of the two hy-

drogens is bent nearly 130° from linearity, while the other hydrogen is bent by less than 2°. For this reason, we expect eigenstates with local bend character to play a special role in promoting acetylene–vinylidene isomerization.

ACKNOWLEDGMENTS

This research has been supported by DOE Grant No. DE-FG0287ER13671. M.P.J. acknowledges support from the Department of the Army under a National Defense Science and Engineering Graduate Fellowship, and from the Fannie and John Hertz Foundation.

[1] M. P. Jacobson, J. P. O'Brien, R. J. Silbey, and R. W. Field, J. Chem. Phys. **109**, 121 (1998).
[2] J. E. Baggott, Mol. Phys. **65**, 739 (1988).
[3] H. Ishikawa, C. Nagao, N. Mikami, and R. W. Field, J. Chem. Phys. **109**, 492 (1998).
[4] R. Marquardt and M. Quack, J. Chem. Phys. **95**, 4854 (1991).
[5] R. Marquardt, M. Quack, J. Stohner, and E. Sutcliffe, J. Chem. Soc., Faraday Trans. 2 **82**, 1173 (1986).
[6] J. P. Rose and M. E. Kellman, J. Chem. Phys. **105**, 10743 (1996).
[7] L. Xiao and M. E. Kellman, J. Chem. Phys. **90**, 6086 (1989).
[8] L. Xiao and M. E. Kellman, J. Chem. Phys. **93**, 5805 (1990).
[9] M. E. Kellman and L. Xiao, J. Chem. Phys. **93**, 5821 (1990).
[10] G. S. Ezra, J. Chem. Phys. **104**, 26 (1996).
[11] M. Joyeux, J. Mol. Spectrosc. **175**, 262 (1996).
[12] J. Main, C. Jung, and H. S. Taylor, J. Chem. Phys. **107**, 6577 (1997).
[13] H.-M. Keller, M. Stumpf, T. Schröder, C. Stöck, F. Temps, R. Schinke, H.-J. Werner, C. Bauer, and P. Romus, J. Chem. Phys. **106**, 5359 (1997).
[14] C. Beck, H.-M. Keller, S. Yu. Grebenschchikov, R. Schinke, S. Farantos, K. Yamashita, and K. Morokuma, J. Chem. Phys. **107**, 9818 (1997).
[15] T. Sako and K. Yamanouchi, Chem. Phys. Lett. **264**, 403 (1997).
[16] F. Iachello and R. D. Levine, *Algebraic Theory of Molecules* (Oxford University Press, New York, 1995).
[17] M. E. Kellman, Annu. Rev. Phys. Chem. **46**, 395 (1995).
[18] F. Perez Bernal, R. Bijker, A. Frank, R. Lemus, and J. M. Arias, Chem. Phys. Lett. **258**, 301 (1996).
[19] M. E. Kellman, J. Chem. Phys. **93**, 6630 (1990).
[20] M. E. Kellman and G. Chen, J. Chem. Phys. **95**, 8671 (1991).
[21] C. Jaffe and M. E. Kellman, J. Chem. Phys. **92**, 7196 (1990).
[22] L. E. Fried and G. S. Ezra, J. Chem. Phys. **86**, 6270 (1987).
[23] J. Manz and H. H. Schor, Chem. Phys. Lett. **107**, 542 (1984).
[24] S. K. Gray and M. S. Child, Mol. Phys. **53**, 961 (1984).
[25] E. J. Heller, E. B. Stechel, and M. J. Davis, J. Chem. Phys. **73**, 4720 (1980).
[26] K. K. Lehmann, J. Chem. Phys. **79**, 1098 (1983).
[27] M. E. Kellman, J. Chem. Phys. **76**, 4528 (1982).
[28] M. E. Kellman, J. Chem. Phys. **83**, 3843 (1985).
[29] I. M. Mills and A. G. Robiette, Mol. Phys. **56**, 743 (1985).
[30] I. M. Mills and F. J. Mompean, Chem. Phys. Lett. **124**, 425 (1986).
[31] K. K. Lehmann, J. Chem. Phys. **84**, 6524 (1986).
[32] R. G. Della Valle, Mol. Phys. **63**, 611 (1988).
[33] R. Mecke, Z. Phys. **81**, 313 (1933).
[34] M. S. Child and R. T. Lawton, Faraday Discuss. **71**, 273 (1981).
[35] R. T. Lawton and M. S. Child, Mol. Phys. **40**, 773 (1980).
[36] B. R. Henry and W. Siebrand, J. Chem. Phys. **49**, 5369 (1968).
[37] W. Siebrand and D. F. Williams, J. Chem. Phys. **49**, 1860 (1968).
[38] M. S. Child and L. Halonen, Adv. Chem. Phys. **57**, 1 (1984).
[39] Y. Osamura, H. F. Schaefer III, S. K. Gray, and W. H. Miller, J. Am. Chem. Soc. **103**, 1904 (1981).
[40] T. Carrington, Jr., L. M. Hubbard, H. F. Schaefer III, and W. H. Miller, J. Chem. Phys. **80**, 4347 (1984).
[41] M. M. Gallo, T. P. Hamilton, and H. F. Schaefer III, J. Am. Chem. Soc. **112**, 8714 (1990).
[42] Y. Chen, D. M. Jonas, J. L. Kinsey, and R. W. Field, J. Chem. Phys. **91**, 3976 (1989).
[43] K. M. Ervin, J. Ho, and W. C. Lineberger, J. Chem. Phys. **91**, 5974 (1989).
[44] J. F. Stanton and J. Gauss, J. Chem. Phys. (to be published).
[45] M. P. Jacobson, C. Jung, H. S. Taylor, and R. W. Field (in preparation).
[46] E. L. Sibert III and R. C. Mayrhofer, J. Chem. Phys. **99**, 937 (1993).
[47] A. B. McCoy and E. L. Sibert III, J. Chem. Phys. **105**, 469 (1996).
[48] E. L. Sibert III, W. P. Reinhardt, and J. T. Hynes, J. Chem. Phys. **77**, 3583 (1982).
[49] E. L. Sibert III, J. T. Hynes, and W. P. Reinhardt, J. Chem. Phys. **77**, 3595 (1982).
[50] G. M. Schmid, S. Coy, R. W. Field, and R. J. Silbey, Chem. Phys. Lett. **219**, 331 (1994).
[51] J. P. O'Brien, M. P. Jacobson, J. J. Sokol, S. L. Coy, and R. W. Field, J. Chem. Phys. **108**, 7100 (1998).
[52] Note that in the absence of rovibronic interactions, l is an *exactly*, as opposed to approximately, conserved quantum number. In our DF spectra, we minimize the effects of rotationally inhomogenous interactions by accessing states with low angular momentum quantum numbers ($J=1$ and 2).
[53] M. Abbouti Temsamani and M. Herman, J. Chem. Phys. **102**, 6371 (1995).
[54] M. Abbouti Temsamani, M. Herman, S. A. B. Solina, J. P. O'Brien, and R. W. Field, J. Chem. Phys. **105**, 11357 (1996).
[55] J. Plíva, J. Mol. Spectrosc. **44**, 165 (1982).
[56] C. Cohen-Tannoudi, B. Diu, and F. Laloë, *Quantum Mechanics* (Wiley, New York, 1977), Vol. 1, pp. 727–741.
[57] Note that the diagonal elements of $H_{\mathcal{N}}^{\text{eff}}$ differ from a standard Dunham expansion in the treatment of zero-point energy; that is, the zero of energy of $H_{\mathcal{N}}^{\text{eff}}$ is defined to be the zero-point level of the molecule, and the ω, x, y, etc. parameters are not the standard Dunham parameters. We have adopted this nonstandard notation for consistency with previous work.
[58] In terms of counting nodes in the (ρ_4,ρ_5) plane, it is important to keep in mind that the radial coordinates are defined only for $\rho \geqslant 0$.
[59] In many local stretching systems, the bottom of a polyad is dominated by local stretch character, whereas the top may remain describable in terms of the normal mode motions. Here, normal mode motions are not in evidence either at the top or the bottom of the polyad.
[60] D. M. Jonas, S. A. B. Solina, B. Rajaram, R. J. Silbey, R. W. Field, K. Yamanouchi, and S. Tsuchiya, J. Chem. Phys. **99**, 7350 (1993).
[61] D. M. Jonas, Ph.D. thesis, Massachusetts Institute of Technology, 1992.
[62] G. Hose and H. S. Taylor, J. Chem. Phys. **76**, 5356 (1982).
[63] Note that these near degeneracies of the local bend eigenstates are predicted by $H_{\mathcal{N}}^{\text{eff}}$ despite the fact that the corresponding g and u symmetry polyads do not even contain the same number of states. For instance, the $[22,0]^{g+}$ polyad contains 42 states, while $[22,0]^{u+}$ contains only 36.
[64] E. L. Sibert III and A. B. McCoy, J. Chem. Phys. **105**, 459 (1996).
[65] K. K. Lehmann, J. Chem. Phys. **96**, 8117 (1992).
[66] This numerical method is analagous to a commonly used procedure for transforming among the various Hund's cases; see R. W. Field and H. Lefebvre-Brion, *Perturbations in the Spectra of Diatomic Molecules* (Academic, Orlando, 1986), pp. 50–51.
[67] These two eigenstates have symmetries of $u/+$ and $u/-$, and both have an energy of 14274.8 cm^{-1}. They also each have 81.4% character of $|11^{+11},11^{-11}\rangle_{\mathcal{N}}$. Thus, the normal mode states with maximal angular momentum associated with the *trans* and *cis* oscillators remain decoupled from the rest of the states; they can be considered ''extreme motion states'' in the normal mode basis.
[68] J. P. Rose and M. E. Kellman, J. Chem. Phys. **105**, 7348 (1996).
[69] M. J. Bramley, S. Carter, N. C. Handy, and I. M. Mills, J. Mol. Spectrosc. **301**, 301 (1993).